7

Dynamic Heterogeneity in Room-Temperature Ionic Liquids

Daun Jeong,[1] Daekeon Kim,[2] M. Y. Choi,[3] Hyung J. Kim,[4] and YounJoon Jung[5*]

[1]*Department of Chemistry, University of California, Irvine, CA 92697*
[2,5]*Department of Chemistry, Seoul National University, Seoul 151-747*
[3]*Department of Physics and Astronomy, Seoul National University, Seoul 151-747*
[4]*Department of Chemistry, Carnegie Mellon University, Pittsburgh, PA 15213*
[1,4]*USA*
[2,3,5]*Korea*

1. Introduction

Room temperature ionic liquids (RTILs) are comprised of bulky organic cations and anions (Holbrey & Seddon, 1999; Weingärtner, 2008). Because of the intricate interplay of various inter- and intramolecular interactions, RTILs have rich dynamical properties and have found diverse applications. In particular, negligible vapor pressure of RTILs makes them a green alternative of conventional organic solvent. For understanding of RTIL's dynamical behavior at the molecular level, solvation and rotational dynamics have been studied experimentally (Arzhantsev et al., 2007; 2006; Cang et al., 2003; Funston et al., 2007; Ingram et al., 2003; Jin et al., 2007; Karmakar & Samanta, 2002a;b; Lang et al., 2006) and theoretically (Jeong et al., 2007; Kobrak, 2006; 2007; Kobrak & Znamenskiy, 2004; Shim et al., 2006; 2007; Shim & Kim, 2009). It is found that the ultrafast relaxation in a subpicosecond time regime contributes substantially to solvation dynamics, disproving the diffusion-controlled solvation in RTILs. On the other hand, in the long time regime, solvation and rotational dynamics of RTILs show slow nonexponential relaxations, which is a characteristic of glassy liquids (Jeong et al., 2008; Shim et al., 2005b).

In this chapter, we particularly focus on the dynamical properties of RTILs as a viscous liquid (Rodriguez & Brennecke, 2006). High viscosity of RTILs has two different aspects in nanoscale applications such as solar cells (Noda et al., 2003; Wang et al., 2003) and capacitors (Tsuda & Hussey, 2007): it is advantageous to preventing the leakage of electrolyte, but disadvantageous to enhancing transport properties. In order to realize the potential applications of RTILs, it is necessary to scrutinize the transport process and relaxation dynamics in RTILs microscopically via molecular dynamics (MD) simulations (Bhargava & Balasubramanian, 2005; Klähn et al., 2008; Popolo & Voth, 2004; Zhao et al., 2009). One notable feature observed in simulation studies of RTILs is so called dynamic heterogeneity (Habasaki

*Corresponding author. E-mail: yjjung@snu.ac.kr

& Ngai, 2008; Hu & Margulis, 2006), which refers to spatially inhomogeneous relaxation behavior (Ediger, 2000; Richert, 2002) in glassy or supercooled liquids (Debenedetti & Stillinger, 2001). Dynamic heterogeneity in RTILs has been observed in the fluorescence spectroscopy experiments (Hu & Margulis, 2006; Samanta, 2006).

In this chapter, we present an overview on our recent MD studies of dynamic heterogeneity of RTILs employing a coarse-grained model of 1-ethyl-3-methylimidazolium hexafluorophsphate ($EMI^+PF_6^-$) (Jeong et al., 2010; Jeong & Jung, 2010; Kim et al., 2010). Dynamic heterogeneity has been investigated numerically in various models of supercooled liquids and glass (Chakrabarti & Bagchi, 2006; Chaudhuri et al., 2007; 2008; Kob et al., 1997; Lačević et al., 2003; Leonard & Berthier, 2005). Regardless of detailed description in modelling, observed in common are the nonexponential relaxation, breakdown of Stokes-Einstein (SE) or Debye-Stokes-Einstein relation, and decoupling of the exchange and persistence times (Hedges et al., 2007; Jung et al., 2004; 2005). Our model of RTILs has molecular interactions which are strikingly different from those in supercooled liquids due to the Coulomb interactions. The dynamical properties mentioned above are also observed similarly in our model and suggested to be essential features of dynamic heterogeneity in RTILs.

The heterogeneity in RTILs may imply structural heterogeneity in mesoscale such as the assembled structure of long alkyl chains (Wang et al., 2007; Wang & Voth, 2005). We point out that the cation in our model employs a united atom description for short alkyl chain. Thus, locally ordered structures and hydrogen bond networks are not expected to appear in our simulation results. However, structural influence on inhomogeneous dynamics is still an intriguing and open question in this simplified model.

This chapter is organized as follows: In Sec. 2, a coarse-grained model of a RTIL is introduced. In Sec. 3, we present the MD results for glassy dynamics. Various dynamic properties manifesting dynamic heterogeneity are demonstrated in Sec. 4, while Sec. 5 is devoted to analyzing the dynamic propensity and Coulomb potential energy. Finally, we conclude in Sec. 6.

2. A coarse-grained model of ionic liquids

We introduce a coarse-grained models to study the dynamics of RTILs via MD simulations covering many orders of magnitude in time scale (Jeong et al., 2010). Fast degrees of freedom which engage the hydrogen atom as well as the vibration of bonds are excluded by employing the united atom representation. Our coarse-grained model is based on the model studied by Kim and coworkers (Shim et al., 2005a). To be specific, the methyl group (M1) and the moieties of the ethyl group (E1, M3) in the cation, EMI^+, were represented by united atoms, using the AMBER force field(Cornell et al., 1995) and the partial charge assignments proposed by Lynden-Bell and cowarkers.(Hanke et al., 2001) The anion PF_6^- was also described as a united atom. One further simplification employed in our model is that five atoms in the imidazole ring and three attached H atoms are represented by a united atom T1 positioned at the center of mass of 8 atoms. The Lennard-Jones (LJ) parameters of T1 were adjusted, so that our model reproduces the liquid structure of the model studied by Kim and coworkers. MD simulations of the coarse-grained model for $EMI^+PF_6^-$ are performed using the DL_POLY program.(Forster & Smith, 2001). Atoms i and j at positions $\mathbf{r}_i$ and $\mathbf{r}_j$ interact with each other through the LJ and Coulomb potentials:

$$U_{ij} = 4\epsilon_{ij}\left[\left(\frac{\sigma_{ij}}{r_{ij}}\right)^{12} - \left(\frac{\sigma_{ij}}{r_{ij}}\right)^{6}\right] + \frac{q_i q_j}{r_{ij}}, \tag{1}$$

atom	σ_{ii} (Å)	ϵ_{ii} (kJ/mol)	q_i (e)	mass (amu)
M1	3.905	0.7330	0.316	15.04092
T1	4.800	1.5000	0.368	67.08860
E1	3.800	0.4943	0.240	14.03298
M3	3.800	0.7540	0.076	15.04092
PF6	5.600	1.6680	-1.000	144.97440

Table 1. The LJ parameters, partial charges, and masses of coarse-grained atoms (Jeong et al., 2010)

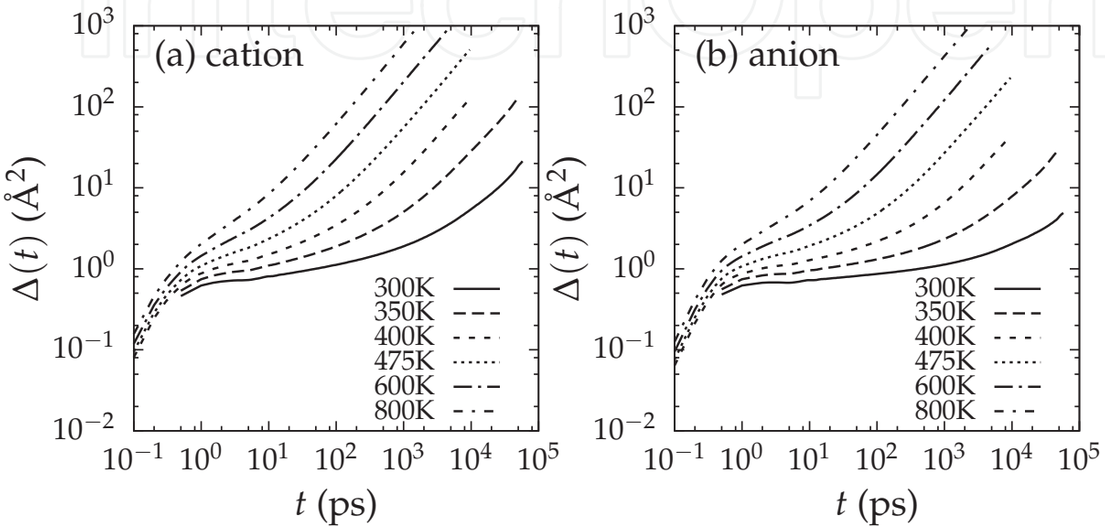

Fig. 1. Mean square displacement of (a) cations and (b) anions at various temperatures.

where $r_{ij} \equiv |\mathbf{r}_i - \mathbf{r}_j|$ is the distance between the two atoms. The parameters of our coarse-grained model are compiled in Table 1.

The model system comprises 512 pairs of rigid cations and anions. We performed simulations in the canonical ensemble using the Nosé-Hoover thermostat and at density $\rho = 1.31\,\mathrm{g/cm^3}$ at six different temperatures. Periodic and cubic boundary conditions were employed and long-range electrostatic interactions were computed via the Ewald method.

3. Glassy dynamics

Glassy dynamics of the coarse-grained RTIL is studied using MD simulation results. We analyze ion diffusion and structural relaxation with the mean square displacement,

$$\Delta(t) = \langle \frac{1}{N} \sum_{i=1}^{N} |\mathbf{r}_i(t) - \mathbf{r}_i(0)|^2 \rangle, \tag{2}$$

and self-intermediate scattering function,

$$F_s(q_0, t) \equiv \langle \frac{1}{N} \sum_{i=1}^{N} e^{i\mathbf{q}_0 \cdot [\mathbf{r}_i(t) - \mathbf{r}_i(0)]} \rangle, \tag{3}$$

where $\langle \cdots \rangle$ denotes the equilibrium ensemble average, N the number of ions, and $\mathbf{q}_0$ the wave vector which corresponds to the position of the first peak in the static structure factor

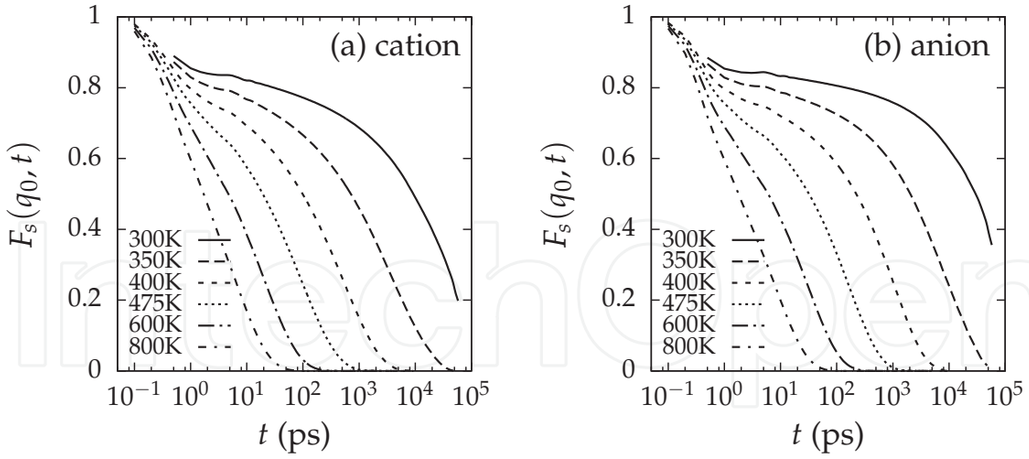

Fig. 2. Self-intermediate scattering function $F_s(q_0,t)$ for (a) cations and (b) anions. The wave vector q_0 is set to 1.24 Å^{-1} in (a) and (b), which corresponds to the position of the first peak in the static structure factor for all ions.

for all ions. In this model, q_0 is found to be 1.24 Å^{-1} regardless of the temperature. It is attributed to the constant density employed in our model, while the density increases slightly in real RTILs and so does q_0, as the temperature is lowered.

In Figs. 1 and 2, the ionic liquid exhibits subdiffusive behavior and nonexponential relaxation more apparently, as the temperature is lowered. $\Delta(t)$ shows sublinear dependence in the intermediate time scale, which is followed by a crossover to Fickian behavior eventually. In the time scale of non-Fickian behavior, we observe the plateau regime (β relaxation) in $F_s(q_0,t)$, while the slow α relaxation follows in the long time regime. The latter is well described by a stretched exponential function, $c\exp[-(t/\tau_0)^\beta]$. At 300 K, the exponent β is found to be 0.64 and 0.59 for cations and anions, respectively, while 0.89 and 0.92 at 800 K. The exponent β being less than unity as well as the subdiffusion and β relaxation is known to be a good indicator of the glassy dynamics. The origin of the stretched exponential relaxation has been discussed to be either the superposition of different exponential relaxations which arise from heterogeneous dynamics or intrinsically nonexponential relaxation (Colmenero et al., 1999).

The structural relaxation time τ_α is determined by the relation $F_s(q_0,\tau_\alpha) = e^{-1}$ using the results in Fig 2. The temperature dependence of τ_α is presented in Fig. 3. We observe that τ_α does not follow the Arrhenius law $\tau_\alpha \propto \exp(d_2/T)$, but rather a super-Arrhenius behavior given by $\tau_\alpha \propto \exp(d_1/T^2)$. This indicates that our model of RTILs belongs to a fragile glass former. A super-Arrhenius behavior in a similar RTIL has been also observed in a recent experiment (Xu et al., 2003) For clarity, we note that we have assumed constant density at all temperatures in our model. If the variation of density were employed, the structural relaxation would be accelerated at high temperatures and decelerated at low temperatures. This would not change the fragile behavior of our model qualitatively.

4. Dynamic heterogeneity

Dynamic heterogeneity of our ionic liquid system is investigated by verifying dynamic correlations between local excitations. We first provide our working definition of local excitations, and present various statistical analyses of them to prove and characterize dynamic heterogeneity.

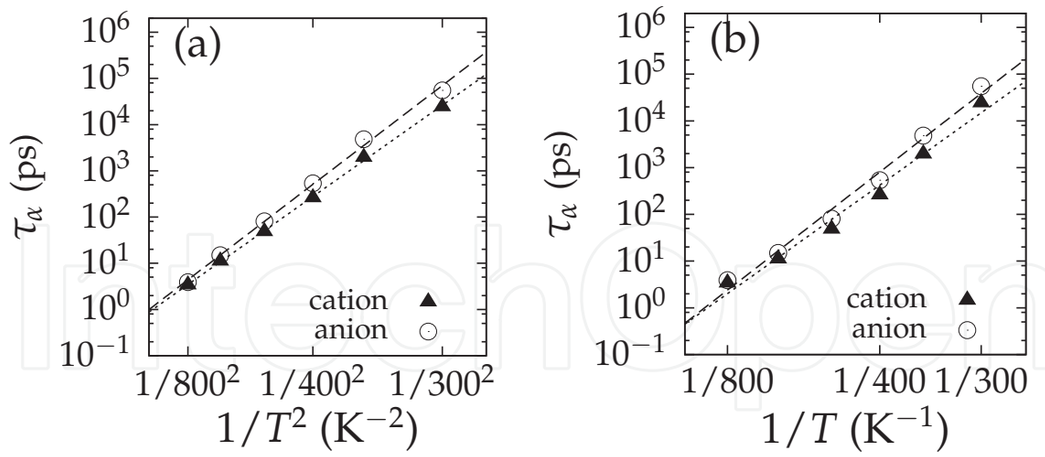

Fig. 3. Temperature dependence of structural relaxation time τ_α (Jeong et al., 2010). Lines are the fitted results using (a) $\tau_\alpha = c_1 \exp(d_1/T^2)$ and (b) $\tau_\alpha = c_2 \exp(d_2/T)$. A super-Arrhenius behavior shown in (a) and (b) suggest that our model of RTILs resembles a fragile glass former.

4.1 Correlated local excitations

A general feature in the diffusive dynamics of supercooled or viscous liquids is that particles are trapped in a cage for a long time because the thermal motions are not activated enough. This is also the case of our model of ionic liquids at low temperatures; an ion exhibits merely oscillatory motions, occasionally interrupted by significant movements. We monitor such large motions of each ion and thereby quantify local dynamics in the ionic liquid. In this study, local excitation events refer to the instances t_1, t_2, t_3, $\cdots$, where the displacement of an ion i exceeds a threshold distance, i.e., $|\mathbf{r}_i(t_1) - \mathbf{r}_i(0)| > d$, $|\mathbf{r}_i(t_2) - \mathbf{r}_i(t_1)| > d$, $|\mathbf{r}_i(t_3) - \mathbf{r}_i(t_2)| > d$, $\cdots$, etc (Hedges et al., 2007). The more local excitation occurs frequently, the more the ion is mobile. The cut off distance d should be chosen appropriately in order to probe the local dynamics. We display the results for $d = 3.0$ Å, for example, and note that other choices of d on the order of the inter-ion distances do not alter our results qualitatively.

An initial excitation of an ion may perturb the local environment and thereby lead to another excitation to the ion or neighboring ions. In the system where the excitations are sparse, the first excitation and subsequent ones indicate different physical circumstances (Jung et al., 2005). The molecular environment providing dynamic constraints persists until the first excitation occurs during fluctuations. Then, the excitation is followed by exchange events due to the dynamic correlations. To verify this, we define the persistence and exchange times to be the waiting times for the first excitation and following ones, and they are denoted by τ_p and τ_x, respectively. The facilitated dynamics would results in the decoupling of the exchange and persistence times. The distributions of persistence and exchange times at various temperature for cations and anions are displayed in Fig. 4. At 800 K, the two distributions almost coincide with each other, while they become separated as T is lowered. The correlated excitations bring about the decoupled distributions. This implies that the excitation events should not belong to the Poisson process.

We remark that the above idea has been originally proposed in the kinetically-constrained model (KCM) (Garrahan & Chandler, 2002), which describes the dynamics of supercooled liquids successfully employing a two-state variable with kinetic constraint. Prior to our study

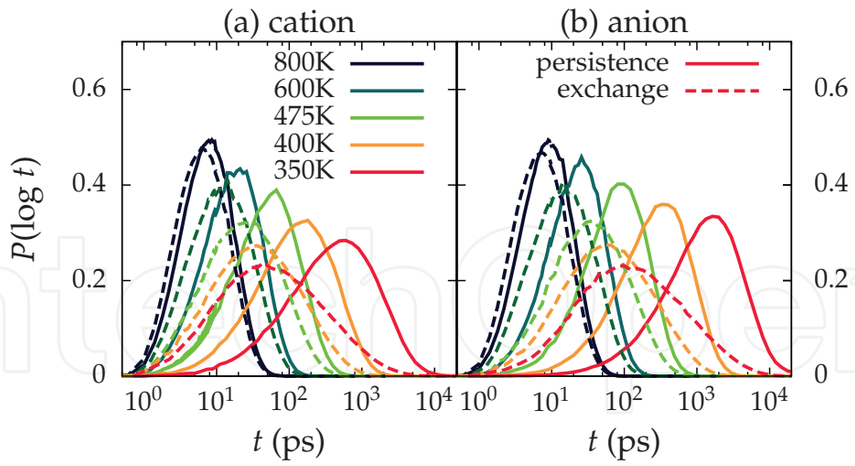

Fig. 4. Decoupling of persistence and exchange times for (a) cations and (b) anions in a coarse-grained model of $EMI^+PF_6^-$ (Jeong et al., 2010).

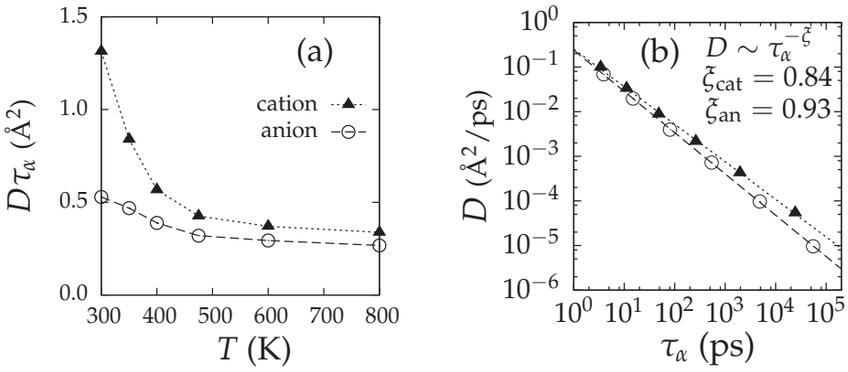

Fig. 5. Violation of the Stokes-Einstein relation in a coarse-grained model of $EMI^+PF_6^-$ (Jeong et al., 2010). (a) As the temperature is lowered, $D\tau_\alpha$ increases. The deviation from a constant is more substantial in case of cations. Lines are guides for the eyes. (b) The exponents in the scaling relation $D \sim \tau_\alpha^{-\xi}$ are found to be 0.84 and 0.93 for cations and anions, respectively, while $\xi = 1$ corresponds to the Stokes-Einstein relation. Lines are the fitted results.

of the ionic liquid, the decoupling of the exchange and persistence times has been shown in not only the KCM but also the WCA model (Hedges et al., 2007), which is an atomistic model for supercooled liquids.

4.2 Violation of Stokes-Einstein relation

The Stokes-Einstein(SE) relation is one of hydrodynamic relations for transport properties. In normal liquids, the relation

$$D \propto \frac{T}{\eta} \tag{4}$$

is usually accurate. In this study, we use another equivalent relation,

$$D \propto \frac{1}{\tau_\alpha}, \tag{5}$$

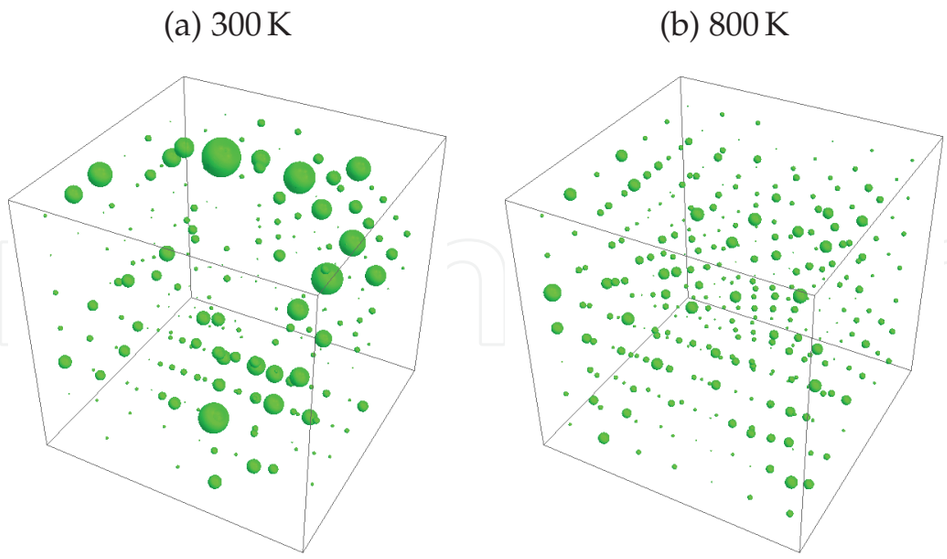

Fig. 6. Spatial heterogeneity of the mobility in a coarse-grained model of $EMI^+PF_6^-$ at (a) 300 K and (b) 800 K. For each cell, the sphere depicts the mobility m_k such that its radius is proportional to m_k.

where τ_α is the structural relaxation time assuming that τ_α is proportional to η/T. We obtain the diffusion constant D from the mean square displacement $\Delta[t-t_0] = \langle N^{-1}\sum_{i=1}^{N}|\mathbf{r}_i(t) - \mathbf{r}_i(t_0)|^2\rangle$, using the relation $\lim_{t\to\infty}\Delta[t-t_0] = 6D(t-t_0)$. At low temperatures, sub-diffusive behavior is pronounced in the intermediate time scale. Thus, we find the time t_0 when the Fickian behavior appears in $\Delta[t-t_0]$ to specify the diffusion regime correctly (Szamel & Flenner, 2006). The structural relaxation time τ_α has been obtained in Sec. 3.
If Equation 5 holds, $D\tau_\alpha$ would be a constant for all temperatures. We display the deviation of $D\tau_\alpha$ for cations and anions in Fig. 5 (a), which means the structural relaxation decouples from diffusive dynamics as T is lowered. To characterize the decoupling behavior in comparison with supercooled liquids, we employ the scaling relation,

$$D \sim \tau_\alpha^{-\xi}, \tag{6}$$

where $\xi = 1$ corresponds to the SE relation. The results $\xi = 0.84$ for cations and 0.93 for anions reveal a relatively weak SE violation in our model (Fig. 5 (b)), compared with supercooled liquids. In the KCM, τ_α corresponds to the average persistence time $\langle\tau_p\rangle$ (Berthier et al., 2005), while the mechanism of self-diffusion is related to the dynamic exchange events. Therefore, the violation of SE relation has a deep connection with the decoupling of the exchange and persistence times. In this sense, the violation of the SE relation is another manifestation of dynamic heterogeneity. It is also noteworthy that the exponent for the cation is less than that for the anion. This indicates that cations should contribute more significantly to the dynamic heterogeneity, which we turn to later.

4.3 Heterogeneity relaxation

We use the excitations defined in Sec. 4.1 to characterize the dynamic heterogeneity by quantifying the local dynamics. We count excitations during a time interval to specify mobile

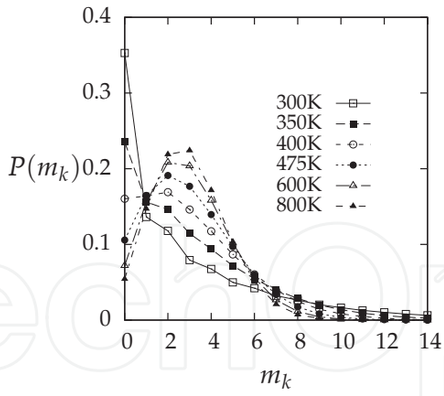

Fig. 7. Probability distributions of m_k at various temperatures.

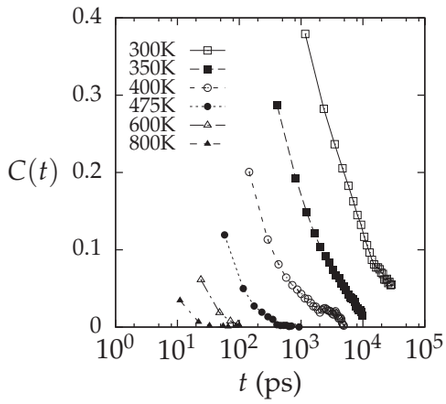

Fig. 8. Time correlation functions of $m_k(t)$ given by Eq. 7.

and immobile regions. The simulation box is divided into $7 \times 7 \times 7$ cells. The mobility $m_k(t)$ is defined to be the number of excitations which occur at time between $t - \tau_{cg}/2$ and $t + \tau_{cg}/2$ in the k-th cell. We hereby obtain the mobility as a function of the position and time which are both coarse-grained. The time interval τ_{cg} is determined to accommodate three excitations on average and depends on the temperature accordingly.

Figure 6 (a) describe the spatial heterogeneity of the mobility at 300 K, where the radius of the spheres centered at the k-th cell is proportional to m_k. We observe the clustering of mobile and immobile regions. In contrast, the mobility appears relatively more homogeneous at 800 K, in Fig. 6 (b). We confirm this by observing the distributions of the mobility in Fig. 7. At 800 K, $P(m_k)$ exhibits a Gaussian distribution. As the temperature is lowered, $P(m_k)$ becomes asymmetric and develops a tail at large m_k demonstrating a clustering of excitations. Note that the the average of m_k over all cells is set to be 3.0 by adjusting τ_{cg}.

The heterogeneity of the mobility is expected to relax with a long time scale. We obtain the time scale of the heterogeneity relaxation by computing the normalized time correlation function given by

$$C(t) \equiv \frac{\langle \overline{m_k(t) m_k(0)} \rangle - \langle \overline{m_k(0)} \rangle^2}{\langle \overline{m_k(0)^2} \rangle - \langle \overline{m_k(0)} \rangle^2}, \tag{7}$$

where the overline and $\langle \cdots \rangle$ denote the averages over k and the equilibrium ensemble, respectively. The results for $C(t)$ at $T = 300 \sim 800$ K are displayed in Fig. 8. $C(t)$ shows rapid decay for $t \lesssim \tau_{cg}$ followed by nonexponential decay thereafter. The characteristic time

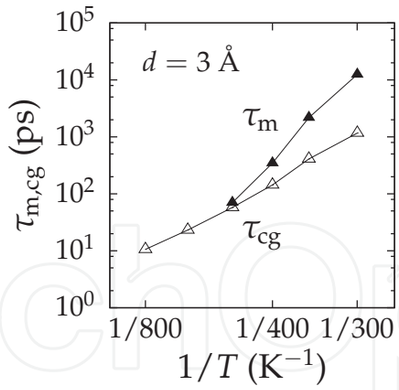

Fig. 9. Temperature dependences of $\tau_{\rm cg}$ and τ_m. $\tau_{\rm cg}$ increases exponentially with the inverse temperature. The time scale τ_m for the mobility relaxation is determined from $C(\tau_m) = 0.1$ displayed in Fig. 8. The increase of τ_m is faster than that of $\tau_{\rm cg}$.

scale τ_m of the heterogeneity is determined by the relation $C(\tau_m) = 0.1$. Figure 9 shows the temperature dependences of τ_m and $\tau_{\rm cg}$. The increase in $\tau_{\rm cg}$ with a decrease in the temperature indicates the slowing down of the dynamics. In particular, τ_m increases faster than that of $\tau_{\rm cg}$ as the temperature is lowered. At low temperatures, the correlation of the mobility maintains for a significantly long time, e.g., about ten nanoseconds at 300 K which is about a hundred times longer than the time interval for measuring the mobility.

5. Structural heterogeneity

Dynamic properties presented in Sec. 4 demonstrate that local dynamic constraint in fluctuation-dominated dynamics is responsible for the dynamic heterogeneity in our coarse-grained ionic liquid. To consider the structural origin producing the dynamic constraint in RTILs, we examine dynamic propensity to probe the role of initial structure in Sec. 5.1. Then, we analyze the Coulomb potential energy which represent the heterogeneous structures of RTILs in Sec. 5.2.

5.1 Dynamic propensity

Dynamic propensity has been introduced to study structural influences on the heterogeneous dynamics of supercooled liquids (Rodriguez Fris et al., 2009; Widmer-Cooper & Harrowell, 2007; Widmer-Cooper et al., 2004). Dynamic propensity of the ion i, denoted by p_i, is defined as the mean squared displacement of the ion i for t^*, which is averaged over the trajectories starting from a given initial configuration with different initial momenta, i.e., the isoconfigurational (IC) ensemble,

$$p_i \equiv \langle |\mathbf{r}_i(t^*) - \mathbf{r}_i(0)|^2 \rangle_{\rm IC}. \tag{8}$$

The initial configuration is taken from the equilibrium ensemble and the initial momenta are chosen to follow the Maxwell-Boltzmann distribution corresponding to the temperature. In this study, we repeat simulations 200 times for each initial structure. The time interval t^* is chosen to be $1.5\tau_\alpha$ at each temperature, where τ_α's have been determined in Sec. 3. The averages over the IC ensemble exclude the influence of the direction and magnitude of initial momenta on the resultant dynamics. Thus, p_i would reveal how the ion i tends to be mobile, resulted by, if any, the initial configuration. Previous studies of supercooled liquids

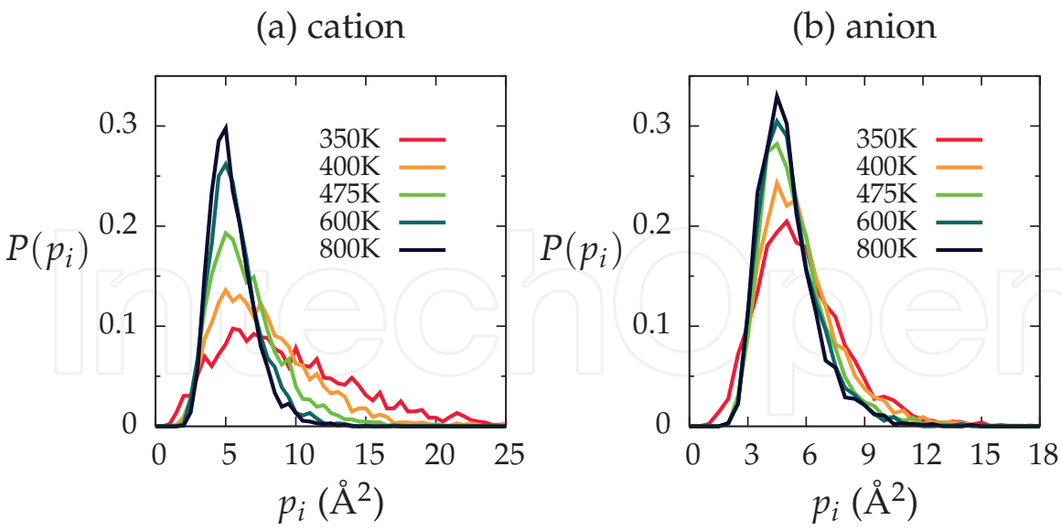

Fig. 10. Probability distributions of dynamic propensity in a coarse-grained model of $EMI^+PF_6^-$ for (a) cations and (b) anions.

have found that several local structural quantities and the potential energy do not have any direct correlations with the propensity of individual particle, but a general overlap of spatial distributions in a large lengh scale (Berthier & Jack, 2007; Widmer-Cooper & Harrowell, 2006; Widmer-Cooper et al., 2004; 2008).

Figure 10 shows the probability distributions $P(p_i)$ of dynamic propensities for cations and anions at five temperatures. The distributions are obtained by performing averages over the results from five uncorrelated initial configurations at each temperature. At 800 K, the highest temperature we studied, $P(p_i)$ follow a narrow Gaussian distribution for both cations and anions. As the temperature is lowered, $P(p_i)$ becomes more broad and asymmetric. The Gaussian shape of $P(p_i)$ implies that each ion has an identical environment statistically for t^* according to the central limit theorem. Thus, a substantial deviation from the Gaussian distribution means that each ion is located in heterogeneous environments. Though not specified yet, there might be relatively more restrictive structures resulting in small propensity, while less restrictive structures facilitate large propensity. Thus, the change of the distributions with the decrease of the temperature indicates the development of the dynamic heterogeneity.

One interesting feature in Fig. 10 is that the tails of $P(p_i)$ at large propensity become more distinct in case of the cations, as the temperature is lowered. It implies that cations make more dominant contributions to the heterogeneous dynamics in our model. In Sec. 3, we have observed that τ_α for anions is much longer than that of cations, especially at low temperatures, and so is t^*. Therefore, most of surrounding cations for an anion undergo complete structural relaxation, resulting in relatively homogeneous environment for the anion. It is consistent with the result in Sec. 4.2, where the breakdown of SE relation is prominent in case of cations.

5.2 Coulomb potential energy

To examine a heterogeneous enviornment which may affects motions of individual ion, we calculate the Coulomb potential energy U_i at the position of the ion i using the Ewald

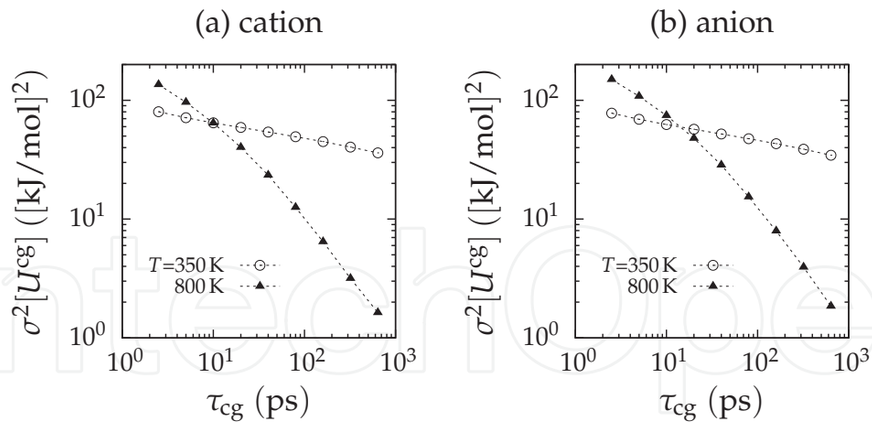

Fig. 11. The variance of U_i^{cg} for (a) cations and (b) anions versus τ_{cg}, where U_i^{cg} is obtained using Eq. 10 for each τ_{cg}.

method (Forster & Smith, 2001),

$$U_i = \sum_{\mathbf{k}\neq 0}\sum_{j=1}^{N} \frac{4\pi q_i q_j}{k^2} \exp[i\mathbf{k}\cdot(\mathbf{r}_i - \mathbf{r}_j)] \exp(-k^2/4\alpha) + \sum_{j(\neq i)} \frac{q_i q_j}{|\mathbf{r}_i - \mathbf{r}_j|} \mathrm{erfc}(\sqrt{\alpha}|\mathbf{r}_i - \mathbf{r}_j|), \quad (9)$$

where q_i is the charge of the ion i and α is a parameter which determines a Gaussian distribution for screening and compensating charges in the Ewald method.
Due to the inertial dynamics of ions, U_i fluctuates with large amplitude. We take average of U_i during a coarse-graining time interval τ_{cg} to probe only the structural aspect. The coarse-grained Coulomb potential energy for the ion i is given by

$$U_i^{cg}(t) \equiv \frac{1}{\tau_{cg}} \int_{t-\tau_{cg}/2}^{t+\tau_{cg}/2} U_i(t')dt'. \quad (10)$$

We study how the distribution of U_i^{cg} depends on τ_{cg} here. With the increase of τ_{cg}, the variance of U_i^{cg} over ions, $\sigma^2[U^{cg}]$, should decrease in general. However, Figure 11 shows that $\sigma^2[U^{cg}]$ does not decrease substantially as τ_{cg} increases at a low temperature 350 K. It is because the values of τ_{cg} employed in Fig. 11 are shorter than the structural relaxation time τ_α, which are found to be 1960 ps and 4840 ps for cations and anions, respectively, in Sec. 3. On the other hand, $\sigma^2[U^{cg}]$ decreases faster at $T = 800$ K, where τ_α are 3.4 ps for cations and 3.9 ps for anions. Specifically, the variance scales as $\sigma[U^{cg}] \sim \tau_{cg}^{-1}$ at 800 K, as it should be when U_i^{cg} follows an identical distribution for all i, according to the central limit theorem. We thus consider the weak decreasing of $\sigma^2[U^{cg}]$ with τ_{cg} at 350 K as a result of heterogeneous structures. If we further increase τ_{cg} to the time much longer than τ_α, $\sigma^2[U^{cg}]$ would start to decrease substantially, and the heterogeneity would be averaged out, eventually. On this account, we consider U_i^{cg} as a quantity which has structural information for individual ion at a low temperature.
To verify the environment which facilitates ions to be mobile or immobile, we consider U_i^{cg} and the mobility m_i, which is defined as the number of excitations of the ion i during τ_{cg}. We obtain conditional probability distributions of U_i^{cg} on the conditions that the ion i has the mobility m_i larger and smaller than m_c. At 300 K, τ_{cg} are set to be 1 ns and 2.5 ns for cations and anions, respectively, while 15 ps and 18 ps at 800 K. We choose $m_c = 2$ for cations

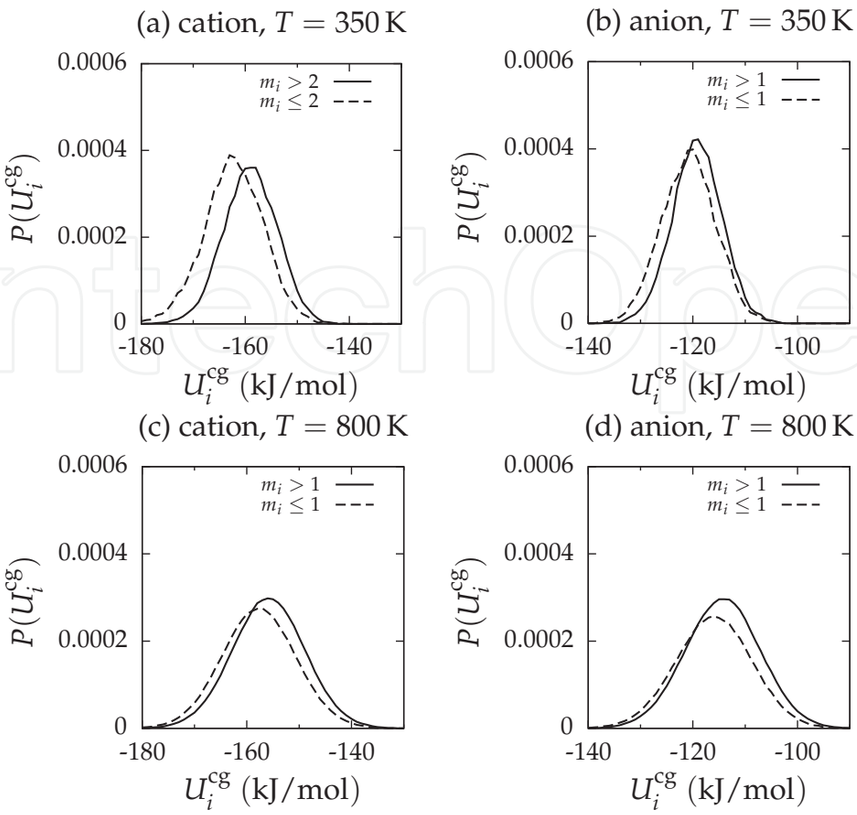

Fig. 12. Conditional probability distributions for U_i^{cg} corresponding to the cases of $m_i > m_c$ and $m_i \leq m_c$ for (a) cations at 350 K, (b) anions at 350 K, (c) cations at 800 K, and (d) anions at 800 K. The coarse-graining time intervals τ_{cg} to obtain U_i^{cg} and m_i are chosen to be 1 ns and 2.5 ns for cations and anions at 350 K, respectively, while τ_{cg} is determined to be 15 ps for cations and 18 ps for anions at 800 K. $m_c = 1$ in (b),(c), and (d), while $m_c = 2$ in (a).

at 350 K, otherwise, $m_c = 1$. In Fig. 12, the conditional probability distributions for $m_i > m_c$ are observed to shift to higher energies for all cases. We first point out that mobile ions have higher U_i^{cg} on average at 800 K as well as 350 K. At 800 K, we have not observed the heterogeneity of m_i or U_i^{cg} which persists significantly. Therefore, higher mobility would not be facilitated by higher U_i^{cg}. It is conjectured that the shift of $P(U_i^{cg})$ should be mainly attributed to the perturbed structures caused by local excitations. Moreover, two distributions exhibit considerable overlaps. Ions can have relatively lower U_i^{cg} even though the ions are mobile in a variety of situations made by complicated dynamics in liquids. In this sense, larger values of U_i^{cg} cannot be a decisive factor to make the ion mobile. However, we also observe more distinct discrepancy between two distributions for cations at 350 K in Fig. 12 (a), compared to other cases. This might be a contribution from heterogeneous structures, which will be specified further in detail as a future study. It is also necessary to examine if these structures act as mobile or immobile environments.

6. Conclusions

To summarize the chapter, we have shown various dynamic properties manifesting the dynamic heterogeneity in a coarse-grained model of $EMI^+PF_6^-$. As the temperature is

lowered, our model system exhibits nonexponential relaxation, subdiffusive behavior, the breakdown of the Stokes-Einstein relation, and the decoupling of persistence and exchange times. We point out that all the properties have been observed in models of supercooled liquids before. The dynamical similarity regardless of strikingly different molecular details is of particular interest. We essentially attribute the universality to the dynamic correlations existed in glassy liquids. Furthermore, the dynamic heterogeneity of our model have been verified by introducing the mobiity, which we claim a convenient quantity to describe local dynamic states. We have also studied how the dynamic correlations are developed, specifically whether they are structurally originated, by computing the dynamic propensity and Coulomb potential energy. In conclusion, the dynamic propensity and Coulomb potential energy demonstrate the dynamic heterogeneity well. However, they do not seem to affect the dynamics decisively. The dynamics of RTILs resolve itself into the fluctuation-dominated dynamics. Nevertheless, it is still necessary to improve microscopic understanding of the diffusion mechanism in terms of the Coulomb interactions. More detailed analyses on the Coulomb potential energy are in progress.

7. Acknowledgements

This work was supported by the National Research Foundation of Korea (Grant Nos. 2010-0001631, 2010-0015243, and 2010-0014525), the KISTI Supercomputing Center (KSC-2009-502-0003), and the BK21 Program.

8. References

Arzhantsev, S., Jin, H., Baker, G. A. & Maroncelli, M. (2007). Measurements of the complete solvation response in ionic liquids, *J. Phys. Chem. B* 111(18): 4978–4989.

Arzhantsev, S., Jin, H., Ito, N. & Maroncelli, M. (2006). Observing the complete solvation response of DCS in imidazolium. ionic liquids, from the femtosecond to nanosecond regimes, *Chem. Phys. Lett.* 417(4-6): 524–529.

Berthier, L., Chandler, D. & Garrahan, J. (2005). Length scale for the onset of Fickian diffusion in supercooled liquids, *Europhys. Lett.* 69(3): 320–326.

Berthier, L. & Jack, R. L. (2007). Structure and dynamics of glass formers: Predictability at large length scales, *Phys. Rev. E* 76(4): 041509.

Bhargava, B. & Balasubramanian, S. (2005). Dynamics in a room-temperature ionic liquid: A computer simulation study of 1,3-dimethylimidazolium chloride, *J. Chem. Phys.* 123(14): 144505.

Cang, H., Li, J. & Fayer, M. (2003). Orientational dynamics of the ionic organic liquid 1-ethyl-3-methylimidazolium nitrate, *J. Chem. Phys.* 119(24): 13017–13023.

Chakrabarti, D. & Bagchi, B. (2006). Decoupling phenomena in supercooled liquids: Signatures in the energy landscape, *Phys. Rev. Lett.* 96(18): 187801.

Chaudhuri, P., Berthier, L. & Kob, W. (2007). Universal nature of particle displacements close to glass and jamming transitions, *Phys. Rev. Lett.* 99(6): 060604.

Chaudhuri, P., Karmakar, S. & Dasgupta, C. (2008). Signatures of dynamical heterogeneity in the structure of glassy free-energy minima, *Phys. Rev. Lett.* 100(12): 125701.

Colmenero, J., Arbe, A., Alegría, A., Monkenbusch, M. & Richter, D. (1999). On the origin of the non-exponential behaviour of the-relaxation in glass-forming polymers: Incoherent neutron scattering and dielectric relaxation results, *J. Phys.:Condens. Matter* 11: A363–A370.

Cornell, W., Cieplak, P., Bayly, C., Gould, I., Merz, K., Ferguson, D., Spellmeyer, D., Fox, T., Caldwell, J. & Kollman, P. (1995). A second generation force field for the simulation of proteins, nucleic acids, and organic molecules, *J. Am. Chem. Soc.* 117(19): 5179–5197.

Debenedetti, P. & Stillinger, F. (2001). Supercooled liquids and the glass transition, *Nature* 410(6825): 259–267.

Ediger, M. (2000). Spatially heterogeneous dynamics in supercooled liquids, *Annu. Rev. Phys. Chem.* 51: 99–128.

Forster, T. R. & Smith, W. (2001). *The DL_POLY-2.13 Reference Manual*, Daresbury Laboratory, Warington, CCLRC.

Funston, A. M., Fadeeva, T. A., Wishart, J. F. & Castner, E. W. (2007). Fluorescence probing of temperature-dependent dynamics and friction in ionic liquid local environments, *J. Phys. Chem. B* 111(18): 4963–4977.

Garrahan, J. & Chandler, D. (2002). Geometrical explanation and scaling of dynamical heterogeneities in glass forming systems, *Phys. Rev. Lett.* 89(3): 035704.

Habasaki, J. & Ngai, K. (2008). Heterogeneous dynamics of ionic liquids from molecular dynamics simulations, *J. Chem. Phys.* 129(19): 194501.

Hanke, C., Price, S. & Lynden-Bell, R. (2001). Intermolecular potentials for simulations of liquid imidazolium salts, *Mol. Phys.* 99(10): 801–809.

Hedges, L. O., Maibaum, L., Chandler, D. & Garrahan, J. P. (2007). Decoupling of exchange and persistence times in atomistic models of glass formers, *J. Chem. Phys.* 127(21): 211101.

Holbrey, J. & Seddon, K. (1999). Ionic liquids, *Clean Products and Processes* 1: 223–236.

Hu, Z. & Margulis, C. (2006). Heterogeneity in a room-temperature ionic liquid: Persistent local environments and the red-edge effect, *Proc. Natl. Acad. Sci. USA* 103(4): 831–836.

Ingram, J., Moog, R., Ito, N., Biswas, R. & Maroncelli, M. (2003). Solute rotation and solvation dynamics in a room-temperature ionic liquid, *J. Phys. Chem. B* 107(24): 5926–5932.

Jeong, D., Choi, M., Jung, Y. & Kim, H. (2008). 1/f spectrum and memory function analysis of solvation dynamics in a room-temperature ionic liquid, *J. Chem. Phys.* 128(17): 174504.

Jeong, D., Choi, M., Kim, H. & Jung, Y. (2010). Fragility, Stokes–Einstein violation, and correlated local excitations in a coarse-grained model of an ionic liquid, *Phys. Chem. Chem. Phys.* 12: 2001–2010.

Jeong, D. & Jung, Y. (2010). Role of the Coulomb interaction in the heterogeneous dynamics of an ionic liquid, *in preparation* .

Jeong, D., Shim, Y., Choi, M. & Kim, H. (2007). Effects of solute electronic polarizability on solvation in a room-temperature ionic liquid, *J. Phys. Chem. B* 111(18): 4920–4925.

Jin, H., Baker, G. A., Arzhantsev, S., Dong, J. & Maroncelli, M. (2007). Solvation and rotational dynamics of coumarin 153 in ionic liquids: Comparisons to conventional solvents, *J. Phys. Chem. B* 111(25): 7291–7302.

Jung, Y., Garrahan, J. & Chandler, D. (2004). Excitation lines and the breakdown of Stokes-Einstein relations in supercooled liquids, *Phys. Rev. E* 69(6): 061205.

Jung, Y., Garrahan, J. & Chandler, D. (2005). Dynamical exchanges in facilitated models of supercooled liquids, *J. Chem. Phys.* 123(8): 084509.

Karmakar, R. & Samanta, A. (2002a). Solvation dynamics of coumarin-153 in a room-temperature ionic liquid, *J. Phys. Chem. A* 106(18): 4447–4452.

Karmakar, R. & Samanta, A. (2002b). Steady-state and time-resolved fluorescence behavior of C153 and PRODAN in room-temperature ionic liquids, *J. Phys. Chem. A* 106(28): 6670–6675.

Kim, D., Jeong, D. & Jung, Y. (2010). Dynamic propensity as an indicator of heterogeneity in room-temperature ionic liquids, *in preparation* .

Klähn, M., Seduraman, A. & Wu, P. (2008). A model for self-diffusion of guanidinium-based ionic liquids: A molecular simulation study, *J. Phys. Chem. B* 112(44): 13849–13861.

Kob, W., Donati, C., Plimpton, S., Poole, P. & Glotzer, S. (1997). Dynamical heterogeneities in a supercooled Lennard-Jones liquid, *Phys. Rev. Lett.* 79(15): 2827–2830.

Kobrak, M. N. (2006). Characterization of the solvation dynamics of an ionic liquid via molecular dynamics simulation, *J. Chem. Phys.* 125(6): 064502.

Kobrak, M. N. (2007). A comparative study of solvation dynamics in room-temperature ionic liquids, *J. Chem. Phys.* 127(18): 184507.

Kobrak, M. & Znamenskiy, V. (2004). Solvation dynamics of room-temperature ionic liquids: Evidence for collective solvent motion on sub-picosecond timescales, *Chem. Phys. Lett.* 395(1-3): 127–132.

Lačević, N., Starr, F., Schrøder, T. & Glotzer, S. (2003). Spatially heterogeneous dynamics investigated via a time-dependent four-point density correlation function, *J. Chem. Phys.* 119(14): 7372.

Lang, B., Angulo, G. & Vauthey, E. (2006). Ultrafast solvation dynamics of coumarin 153 in imidazolium-based ionic liquids, *J. Phys. Chem. A* 110(22): 7028–7034.

Leonard, S. & Berthier, L. (2005). Lifetime of dynamic heterogeneity in strong and fragile kinetically constrained spin models, *J. Phys.:Condens. Matter* 17(45): S3571–S3577.

Noda, A., Susan, M. A. B. H., Kudo, K., Mitsushima, S., Hayamizu, K. & Watanabe, M. (2003). Brønsted acid-base ionic liquids as proton-conducting nonaqueous electrolytes, *J. Phys. Chem. B* 107(17): 4024–4033.

Popolo, M. D. & Voth, G. (2004). On the structure and dynamics of ionic liquids, *J. Phys. Chem. B* 108(5): 1744–1752.

Richert, R. (2002). Heterogeneous dynamics in liquids: Fluctuations in space and time, *J. Phys.:Condens. Matter* 14(23): R703–R738.

Rodriguez, H. & Brennecke, J. (2006). Temperature and composition dependence of the density and viscosity of binary mixtures of water + ionic liquid, *J. Chem. Eng. Data* 51(6): 2145–2155.

Rodriguez Fris, J. A., Alarcon, L. M. & Appignanesi, G. A. (2009). Time evolution of dynamic propensity in a model glass former: The interplay between structure and dynamics, *J. Chem. Phys.* 130(2): 024108.

Samanta, A. (2006). Dynamic Stokes shift and excitation wavelength dependent fluorescence of dipolar molecules in room temperature ionic liquids, *J. Phys. Chem. B* 110(28): 13704–13716.

Shim, Y., Choi, M. & Kim, H. (2005a). A molecular dynamics computer simulation study of room-temperature ionic liquids. I. Equilibrium solvation structure and free energetics, *J. Chem. Phys.* 122(4): 044510.

Shim, Y., Choi, M. & Kim, H. (2005b). A molecular dynamics computer simulation study of room-temperature ionic liquids. II. Equilibrium and nonequilibrium solvation dynamics, *J. Chem. Phys.* 122(4): 044511.

Shim, Y., Jeong, D., Choi, M. & Kim, H. (2006). Rotational dynamics of a diatomic solute in the room-temperature ionic liquid 1-ethyl-3-methylimidazolium hexafluorophosphate, *J. Chem. Phys.* 125(6): 061102.

Shim, Y., Jeong, D., Manjari, S., Choi, M. Y. & Kim, H. J. (2007). Solvation, solute rotation and vibration relaxation, and electron-transfer reactions in room-temperature ionic liquids, *Acc. Chem. Res.* 40(11): 1130–1137.

Shim, Y. & Kim, H. (2009). Adiabatic electron transfer in a room-temperature ionic liquid: Reaction dynamics and kinetics, *J. Phys. Chem. B* 113(39): 12964–12972.

Szamel, G. & Flenner, E. (2006). Time scale for the onset of Fickian diffusion in supercooled liquids, *Phys. Rev. E* 73(1): 11504.

Tsuda, T. & Hussey, C. L. (2007). Electrochemical applications of room-temperature ionic liquids, *Interface* 16: 42–49.

Wang, P., Zakeeruddin, S., Moser, J. & Gratzel, M. (2003). A new ionic liquid electrolyte enhances the conversion efficiency of dye-sensitized solar cells, *J. Phys. Chem. B* 107(48): 13280–13285.

Wang, Y., Jiang, W., Yan, T. & Voth, G. A. (2007). Understanding ionic liquids through atomistic and coarse-grained molecular dynamics simulations, *Acc. Chem. Res.* 40(11): 1193–1199.

Wang, Y. & Voth, G. (2005). Unique spatial heterogeneity in ionic liquids, *J. Am. Chem. Soc.* 127(35): 12192–12193.

Weingärtner, H. (2008). Understanding ionic liquids at the molecular level: Facts, problems, and controversies, *Angew. Chem. Int. Ed.* 47(4): 654–670.

Widmer-Cooper, A. & Harrowell, P. (2006). Predicting the long-time dynamic heterogeneity in a supercooled liquid on the basis of short-time heterogeneities, *Phys. Rev. Lett.* 96(18): 185701.

Widmer-Cooper, A. & Harrowell, P. (2007). On the study of collective dynamics in supercooled liquids through the statistics of the isoconfigurational ensemble, *J. Chem. Phys.* 126(15): 154503.

Widmer-Cooper, A., Harrowell, P. & Fynewever, H. (2004). How reproducible are dynamic heterogeneities in a supercooled liquid?, *Phys. Rev. Lett.* 93(13): 135701.

Widmer-Cooper, A., Perry, H., Harrowell, P. & Reichman, D. R. (2008). Irreversible reorganization in a supercooled liquid originates from localized soft modes, *Nature Physics* 4(9): 711–715.

Xu, W., Cooper, E. & Angell, C. (2003). Ionic liquids: Ion mobilities, glass temperatures, and fragilities, *J. Phys. Chem. B* 107(25): 6170–6178.

Zhao, W., Leroy, F., Heggen, B., Zahn, S., Kirchner, B., Balasubramanian, S. & Müller-Plathe, F. (2009). Are there stable ion-pairs in room-temperature ionic liquids? molecular dynamics simulations of 1-n-butyl-3-methylimidazolium hexafluorophosphate, *J. Am. Chem. Soc.* 131(43): 15825–15833.

Ionic Liquids: Theory, Properties, New Approaches

Edited by Prof. Alexander Kokorin

ISBN 978-953-307-349-1
Hard cover, 738 pages
Publisher InTech
Published online 28, February, 2011
Published in print edition February, 2011

Ionic Liquids (ILs) are one of the most interesting and rapidly developing areas of modern physical chemistry, technologies and engineering. This book, consisting of 29 chapters gathered in 4 sections, reviews in detail and compiles information about some important physical-chemical properties of ILs and new practical approaches. This is the first book of a series of forthcoming publications on this field by this publisher. The first volume covers some aspects of synthesis, isolation, production, modification, the analysis methods and modeling to reveal the structures and properties of some room temperature ILs, as well as their new possible applications. The book will be of help to chemists, physicists, biologists, technologists and other experts in a variety of disciplines, both academic and industrial, as well as to students and PhD students. It may help to promote the progress in ILs development also.

InTech Europe
University Campus STeP Ri
Slavka Krautzeka 83/A
51000 Rijeka, Croatia
Phone: +385 (51) 770 447
Fax: +385 (51) 686 166
www.intechopen.com

InTech China
Unit 405, Office Block, Hotel Equatorial Shanghai
No.65, Yan An Road (West), Shanghai, 200040, China
中国上海市延安西路65号上海国际贵都大饭店办公楼405单元
Phone: +86-21-62489820
Fax: +86-21-62489821

IntechOpen